Acta Applicandae Mathematicae (2024) 190:10
https://doi.org/10.1007/s10440-024-00647-0

Efficient Numerical Schemes for a Two-Species Keller-Segel Model and Investigation of Its Blowup Phenomena in 3D

Xueling Huang[1] · **Jie Shen**[2]

Received: 1 October 2023 / Accepted: 28 March 2024

Abstract
We consider in this paper numerical approximation and simulation of a two-species Keller-Segel model. The model enjoys an energy dissipation law, mass conservation and bound or positivity preserving for the population density of two species. We construct a class of very efficient numerical schemes based on the generalized scalar auxiliary variable with relaxation which preserve unconditionally the essential properties of the model at the discrete level. We conduct a sequence of numerical tests to validate the properties of these schemes, and to study the blow-up phenomena of the model in a three-dimensional domain in parabolic-elliptic form and parabolic-parabolic form.

Keywords Two-species Keller-Segel model · Bound/positivity preserving · Energy dissipation · Blow-up

Mathematics Subject Classification 92C17 · 65M12 · 65M70 · 35Q35

1 Introduction

We consider in this paper the following Keller-Segel (KS) model [2, 28] involving two chemotactic species and a chemoattractant

$$\frac{\partial \rho_1}{\partial t} = \kappa_1 \Delta \rho_1 - \chi_1 \nabla \cdot (\eta(\rho_1) \nabla c), \qquad \boldsymbol{x} \in \Omega,\ t \in (0, T], \tag{1.1}$$

$$\frac{\partial \rho_2}{\partial t} = \kappa_2 \Delta \rho_2 - \chi_2 \nabla \cdot (\eta(\rho_2) \nabla c), \qquad \boldsymbol{x} \in \Omega,\ t \in (0, T], \tag{1.2}$$

Dedicated to Professor Shi Jin's 60th Birthday

✉ J. Shen
jshen@eitech.edu.cn

X. Huang
hxlmath@163.com

[1] School of Mathematical Sciences and Fujian Provincial Key Laboratory on Mathematical Modeling and High Performance Scientific Computing, Xiamen University, Xiamen, Fujian, 361005, China

[2] Eastern Institute for Advanced Study, Eastern Institute of Technology, Ningbo, Zhejiang 315200, P.R. China

Published online: 10 April 2024

$$\tau \frac{\partial c}{\partial t} = \beta \Delta c - \alpha c + \gamma_1 \rho_1 + \gamma_2 \rho_2, \qquad \boldsymbol{x} \in \Omega,\ t \in (0, T], \tag{1.3}$$

subjected to suitable initial conditions

$$\rho_1|_{t=0} = \rho_{10}, \quad \rho_2|_{t=0} = \rho_{20}, \quad c|_{t=0} = c_0, \tag{1.4}$$

in a three-dimensional (3D) bounded domain $\Omega \subset \mathbb{R}^3$ with either

- periodic boundary conditions; or
- no-flux boundary condition on ρ_1, ρ_2, and Neumann boundary condition on c, i.e.,

$$\kappa_1 \frac{\partial \rho_1}{\partial \mathbf{n}} - \chi_1 \eta(\rho_1) \frac{\partial c}{\partial \mathbf{n}} = 0, \quad \kappa_2 \frac{\partial \rho_2}{\partial \mathbf{n}} - \chi_2 \eta(\rho_2) \frac{\partial c}{\partial \mathbf{n}} = 0, \quad \frac{\partial c}{\partial \mathbf{n}} = 0, \tag{1.5}$$

where $\mathbf{n}$ is the outward unit-normal to the boundary $\partial\Omega$.

In the above, functions $\rho_1 = \rho_1(x, y, z, t)$ and $\rho_2 = \rho_2(x, y, z, t)$ denote population density of the two species, $c = c(x, y, z, t)$ is the concentration of a chemoattractant which attracts the two species, and the function $\eta(\rho_i) \geq 0$ with $\eta(0) = 0$ describes the concentration-dependent mobility. Unless stated otherwise, we set $\eta(\rho_i) = \rho_i$ $(i = 1, 2)$. Parameters κ_1, κ_2, β are positive diffusion coefficients, χ_1 and χ_2 are positive sensitivity coefficients of the two species to the chemoattractant, γ_i $(i = 1, 2)$ represents the production rate of chemoattractant, while $\alpha \geq 0$ is the consumption rate of chemoattractant.

The above model is a parabolic-elliptic system when $\tau = 0$, and a parabolic-parabolic system when $\tau > 0$.[1] The model is an extension of the classical KS model which was first proposed in [25, 30] to describe the movement of cells and organisms in response to the concentration gradient of a chemoattractant. There are abundant researches on the classical KS system as well as its various extensions (see, e.g., [1, 16, 17] and references therein). In particular, the multi-species KS model in [13, 36] describes the chemotaxis of different species living together in a biofilm or a ecosystem.

Many studies have demonstrated multi-species KS systems. Even two species exhibit different behaviours from the single species. For instance, Espejo et al. [10] examined a two-species system with $\tau = 0$, $\kappa_1 = \beta = \gamma_1 = \gamma_2 = 1$ and $\alpha c \equiv 1$, and established conditions for both global existence of solutions and finite time blow-up in a two-dimensional ball with radial symmetry. In a separate study [11], Espejo et al. determined a range of parameters that guarantees simultaneous blow-up for non-radial solutions in the whole space $\mathbb{R}^2$. Conca et al. [7] investigated the two-species model with $\tau = \alpha = 0$ and $\kappa_2 = \beta = \gamma_1 = \gamma_2 = 1$ in $\mathbb{R}^2$ and analyzed conditions on the initial data, without any symmetry assumptions, that lead to blow-up or global existence in time. Later, Espejo et al. [12] improved the global existence results in $\mathbb{R}^2$, and summarized the results for global existence and blow-up in $\mathbb{R}^2$. For higher-dimensional cases, only a few studies have focused on the blow-up solutions of the two-species KS model. Biler et al. [2] studied blow-up properties of the parabolic-elliptic system in $\mathbb{R}^d$ $(d \geq 3)$ with $\tau = \alpha = 0$ and $\beta = \gamma_1 = \gamma_2 = 1$. Li et al. [28] demonstrated that the parabolic-parabolic system with $\tau = \kappa_1 = \kappa_2 = \beta = 1$ for dimension $d \geq 3$ in a ball $\mathbb{R}^d$ with radial initial condition may blow up in finite time.

The blow-up described above can be explained as chemotactic collapse [14], which suggests that, under suitable circumstances, an entire population can concentrate in a single

[1] In the particular case with $\tau = \alpha = 0$, the equation (1.3) should be adjusted to $-\beta \Delta c = \gamma_1 \rho_1 + \gamma_2 \rho_2 - \gamma_1 \langle \rho_1 \rangle - \gamma_2 \langle \rho_2 \rangle$ with $\langle \rho_i \rangle = \frac{1}{|\Omega|} \int_\Omega \rho_i d\boldsymbol{x}$ $(i = 1, 2)$, due to the compatibility with the boundary conditions involved [23, 29].

point within a finite time. Mathematically, this corresponds to the formation of a Dirac delta-type singularity in finite time. However, Velázquez [33] emphasized that blow-up is a property that cannot be expected to take place for the magnitudes that describe the behavior of biological or physical systems. Typically, it does not indicate a real singularity, but rather a change in orders of magnitude of some quantity that characterizes the state of a system. For the classical KS model, the blow-up phenomena have been investigated analytically in, e.g., [3, 8], and numerically in [6, 26] where a series of comparative numerical studies on two-species chemotaxis models were conducted and some open questions related to possible blow-up in 2D domains were addressed. However, very few results, if any, are currently available for simulating blow-up of two-species chemotaxis models in 3D.

Many modifications to the classical KS model have been proposed to eliminate blow-up, such as bounded chemotaxis sensibilities, additional cross-diffusion term, degenerate cell diffusion, and logistic sources [16, 22, 27, 32]. For instance, Hillen et al. [15] assumed that the chemotactic response is switched off at high cell density, which successfully prevented overcrowding of the classical KS model. Their numerical simulations also showed interesting phenomena of pattern formation and stable aggregate formation. Furthermore, numerical studies in [6, 26] indicated that this modification is also effective to prevent blow-up for two-species chemotaxis models in 2D domains. On the other hand, Velázquez [33] introduced a small parameter ϵ and studied the evolution of the solutions of the classical KS model beyond the blow-up time for the limit problem. We are naturally curious whether these modifications will also prevent blow-up of the two-species KS model in 3D.

It is challenging to construct numerical schemes, particularly with higher-order, that preserve essential properties, such as bound/positivity, mass conservation, and energy dissipation, of the KS systems [5, 16–18, 24, 35]. Huang and Shen developed in [19] a new class of bound/positivity preserving and energy stable schemes, which can also be higher-order, by combining generalized SAV (GSAV) approach and the function transform approach. In a earlier work [21], we developed the GSAV approach with relaxation (R-GSAV) [37] and to construct bound/positivity preserving schemes for the one-specie Patlak-Keller-Segel-Navier-Stokes system. The main purposes of this paper are as follows:

1. to extend the schemes proposed in [21] for the Patlak-Keller-Segel-Navier-Stokes system to the 3D two-species KS model (1.1)-(1.5);
2. to apply the proposed numerical scheme to simulate the 3D two-species KS model, verify the accuracy of theoretical results on blow-up in [2, 28], and explore the open question of whether solutions of the 3D parabolic-parabolic model blow up with non-radial initial data; and
3. to explore how the model (1.1)-(1.5) can be reasonably modified to avoid blow-up while still capturing essential chemotaxis phenomena.

The rest of the paper is organized as follows. Section 2 presents some basic properties of the two-species KS model (1.1)-(1.5) and reviews key theoretical results on blow-up in [2, 28]. In Sect. 3, we propose a class of efficient R-GSAV schemes and proves that they satisfy essential properties such as bound/positivity preservation, unconditionally energy dissipation and mass conservation. We conduct in Sect. 4 a series of numerical experiments to validate the accuracy of the proposed schemes and investigate the blow-up phenomena under different scenarios. Some concluding remarks are presented in Sect. 5.

2 Properties of the Two-Species KS Model

We start with some basic properties of the two-species KS model (1.1)-(1.5).

Firstly, we can deduce the mass conservation

$$\frac{d}{dt}\int_\Omega \rho_i d\boldsymbol{x} = 0, \quad i = 1, 2 \tag{2.1}$$

by integrating (1.1) and (1.2) over Ω under either periodic or no-flux boundary conditions.

Secondly, it is easy to show that the two-species KS model is dissipative with the free energy

$$E_{tot}(\rho_1, \rho_2, c) = \int_\Omega \left(\frac{\gamma_1\kappa_1}{\chi_1} f(\rho_1) + \frac{\gamma_2\kappa_2}{\chi_2} f(\rho_2) - \gamma_1\rho_1 c - \gamma_2\rho_2 c + \frac{\beta}{2}|\nabla c|^2 + \frac{\alpha}{2}c^2 \right) d\boldsymbol{x}, \tag{2.2}$$

where the function $f(\rho_i)$ is determined by $f''(\rho_i) = \frac{1}{\eta(\rho_i)}$. As we stated earlier that $\eta(\rho_i) = \rho_i$, we can choose $f(\rho_i) = \rho_i \log \rho_i - \rho_i$ with $\rho_i \in (0, +\infty)$ $(i = 1, 2)$ [31].

Thanks to the identity $\Delta\rho_i = \nabla \cdot (\frac{\nabla f'(\rho_i)}{f''(\rho_i)})$, we can rewrite (1.1)-(1.3) as a gradient flow about (ρ_1, ρ_2, c)

$$\begin{aligned}
\frac{\partial \rho_1}{\partial t} &= \kappa_1 \nabla \cdot \left(\frac{\nabla f'(\rho_1)}{f''(\rho_1)} \right) - \chi_1 \nabla \cdot (\eta(\rho_1)\nabla c) \\
&= \nabla \cdot \left(\eta(\rho_1) \nabla \left(\kappa_1 f'(\rho_1) - \chi_1 c \right) \right) \\
&= \frac{\chi_1}{\gamma_1} \nabla \cdot \left(\eta(\rho_1) \nabla \left(\frac{\gamma_1\kappa_1}{\chi_1} f'(\rho_1) - \gamma_1 c \right) \right) \\
&= \frac{\chi_1}{\gamma_1} \nabla \cdot \left(\eta(\rho_1) \nabla \frac{\delta E_{tot}}{\delta \rho_1} \right),
\end{aligned} \tag{2.3}$$

where $\frac{\delta E_{tot}}{\delta \rho_1} = \frac{\gamma_1\kappa_1}{\chi_1} f'(\rho_1) - \gamma_1 c$. Similarly,

$$\frac{\partial \rho_2}{\partial t} = \frac{\chi_2}{\gamma_2} \nabla \cdot \left(\eta(\rho_2) \nabla \frac{\delta E_{tot}}{\delta \rho_2} \right), \tag{2.4}$$

where $\frac{\delta E_{tot}}{\delta \rho_2} = \frac{\gamma_2\kappa_2}{\chi_2} f'(\rho_2) - \gamma_2 c$. Additionally,

$$\tau \frac{\partial c}{\partial t} = \beta \Delta c - \alpha c + \gamma_1\rho_1 + \gamma_2\rho_2 = -\frac{\delta E_{tot}}{\delta c}. \tag{2.5}$$

Furthermore, taking the inner products of (2.3) with $\frac{\delta E_{tot}}{\delta \rho_1}$, (2.4) with $\frac{\delta E_{tot}}{\delta \rho_2}$ and (2.5) with $\frac{\partial c}{\partial t}$, by equal quantity replacement and integration by parts, we sum up them and obtain the energy dissipative law

$$\frac{dE_{tot}(\rho_1, \rho_2, c)}{dt} = -\int_\Omega \left(\frac{\chi_1}{\gamma_1} \eta(\rho_1) \left(\nabla \frac{\delta E_{tot}}{\delta \rho_1} \right)^2 + \frac{\chi_2}{\gamma_2} \eta(\rho_2) \left(\nabla \frac{\delta E_{tot}}{\delta \rho_2} \right)^2 + \tau \left(\frac{\partial c}{\partial t} \right)^2 \right) d\boldsymbol{x}. \tag{2.6}$$

Now we review some theoretical results on blow-up solutions of the two-species KS model in high-dimensional domains. In [2], the authors derived the blow-up condition of the

parabolic-elliptic two-species KS model with $\tau = \alpha = 0$ and $\beta = \gamma_1 = \gamma_2 = 1$ in $\mathbb{R}^d$ ($d \geq 3$). More precisely, it is shown that if the initial data satisfy the inequality

$$L := \left(\frac{\frac{m_1(0)}{\chi_1} + \frac{m_2(0)}{\chi_2}}{M_1 + M_2} \right)^{\frac{d}{2}-1} < R := \frac{(2\max\{\chi_1, \chi_2\})^{1-\frac{d}{2}}}{2d\sigma_d} \frac{(M_1 + M_2)^2}{\frac{\kappa_1}{\chi_1} M_1 + \frac{\kappa_2}{\chi_2} M_2}, \tag{2.7}$$

then, the solutions ρ_1 and ρ_2 of the model blow up in finite time, in the sense that

$$\lim_{t \to T} \left(\|\rho_1(t)\|_p + \|\rho_2(t)\|_p \right) = \infty \tag{2.8}$$

for some $0 < T < \infty$ and all $p > 1$. In the above, $M_i = \int_{\mathbb{R}^d} \rho_{i0}(x)dx$, $m_i(0) = \int_{\mathbb{R}^d} \rho_{i0} \mid x - x_i \mid^2 dx$, $x_i = \int_{\mathbb{R}^d} x\rho_{i0}dx$ ($i = 1, 2$) and $\sigma_d = \frac{d\pi^{\frac{d}{2}}}{\Gamma(\frac{d}{2}+1)}$ which is associated with the functional solution of Laplace's equation, where ρ_{i0} ($i = 1, 2$) is the initial data in (1.4). It is shown in [28] that the parabolic-parabolic two-species KS model with $\tau = \kappa_1 = \kappa_2 = \beta = 1$ in a ball $B_r \subset \mathbb{R}^d$ ($d \geq 3$) may blow-up in finite time. More precisely, it is proved that for any initial mass $M_i > 0$ ($i = 1, 2$), there exists radial initial data $(\rho_{10}, \rho_{20}, c_0) \in (C^0(\overline{B_r}))^2 \times W^{1,\infty}(B_r)$ such that the corresponding solutions blow up in a finite time, in the sense that

$$\lim_{t \to T} \left(\|\rho_1(t)\|_{L^\infty(B_r)} + \|\rho_2(t)\|_{L^\infty(B_r)} \right) = \infty \tag{2.9}$$

for some $0 < T < \infty$.

It is known that the blow-up phenomena of the one-specie KS model ($\rho_1 = \rho_2 = \rho$) can be prevented by modifying the mobility function $\eta(\rho)$ as follows:

- a bounded mobility modification: $\eta(\rho) = \frac{\rho}{1+\epsilon\rho}$ ($\epsilon > 0$), $f(\rho) = \rho\log\rho - \rho + \frac{\epsilon}{2}\rho^2$ with $\rho \in (0, +\infty)$ [33, 34]; and
- a saturation concentration modification: $\eta(\rho) = \rho(1 - \frac{\rho}{S})$ ($S > 0$), $f(\rho) = \rho\log\rho + (S - \rho)\log(1 - \frac{\rho}{S})$ with $\rho \in (0, S)$ [9, 15].

We will modify the concentration-dependent mobility $\eta(\rho_i) = \rho_i$ in the two-species KS model (1.1)-(1.5) to $\eta(\rho_i) = \frac{\rho_i}{1+\epsilon\rho_i}$ and $\eta(\rho_i) = \rho_i(1 - \frac{\rho_i}{S})$ ($i = 1, 2$), and study whether the blow-up in parabolic-elliptic form and parabolic-parabolic form will be prevented or not.

3 Positivity/Bound Preserving R-GSAV Schemes

We construct below fully decoupled R-GSAV schemes for the two-species KS system (1.1)-(1.5).

Firstly, to preserve the positivity of the population density $\rho_i \in (0, +\infty)$, we use the function transform

$$\rho_i = \exp(v_i), \quad i = 1, 2. \tag{3.1}$$

Substituting the above into (1.1) and (1.2) respectively, we obtain

$$\frac{\partial v_i}{\partial t} = \kappa_i \Delta v_i + \kappa_i |\nabla v_i|^2 - \frac{\chi_i}{\exp(v_i)} \nabla \cdot (\eta(\rho_i)\nabla c), \quad i = 1, 2. \tag{3.2}$$

Remark 3.1 For the modified two-species KS model with $\eta(\rho_i) = \frac{\rho_i}{1+\epsilon\rho_i}$ $(i = 1, 2)$, we can use the same transform (3.1) to preserve positivity. On the other hand, for the modified two-species KS model with $\eta(\rho_i) = \rho_i(1 - \frac{\rho_i}{S})$ $(i = 1, 2)$, we can use the transform

$$\rho_i = \frac{S}{2}\tanh(v_i) + \frac{S}{2}, \quad i = 1, 2. \tag{3.3}$$

to preserve the bound of $\rho_i \in (0, S)$. Substituting (3.3) into (1.1) and (1.2) respectively, we obtain, instead of (3.2), that

$$\frac{\partial v_i}{\partial t} = \kappa_i \Delta v_i + \kappa_i \frac{\tanh''(v_i)}{\tanh'(v_i)}|\nabla v_i|^2 - \frac{2\chi_i}{S\tanh'(v_i)}\nabla\cdot(\eta(\rho_i)\nabla c), \quad i = 1, 2. \tag{3.4}$$

To fix the idea, we consider $\eta(\rho_i) = \rho_i$ below, as other cases can be treated similarly. Following [19, 20], we have $E_{tot}(\rho_1, \rho_2, c) := E_1(\rho_1, \rho_2, c) + E_0(c)$ with

$$E_1(\rho_1, \rho_2, c) := \int_\Omega \left(\frac{\gamma_1\kappa_1}{\chi_1} f(\rho_1) + \frac{\gamma_2\kappa_2}{\chi_2} f(\rho_2) - \gamma_1\rho_1 c - \gamma_2\rho_2 c + \frac{\alpha}{4}c^2\right) d\boldsymbol{x},$$

$$E_0(c) := \int_\Omega \left(\frac{\beta}{2}|\nabla c|^2 + \frac{\alpha}{4}c^2\right) d\boldsymbol{x}.$$

Since $f(\rho_i) = \rho_i\log(\rho_i) - \rho_i$ $(i = 1, 2)$ is strictly convex, the function $E_1(\rho_1, \rho_2, c)$ is bounded from below. Hence, there exists $C_0 > 0$ such that $E_1(\rho_1, \rho_2, c) \geq -C_0 + 1$ for all ρ_1, ρ_2 and c. It is clear that $E_0(c)$ is non-negative. Therefore, $E(\rho_1, \rho_2, c) := E_{tot}(\rho_1, \rho_2, c) + C_0 \geq 1$. We can introduce a SAV

$$r(t) := E(\rho_1, \rho_2, c), \tag{3.5}$$

we expand the system (1.1)-(1.3) after applying the function transform (3.1) for the two species ρ_1 and ρ_2 and introducing the SAV $r(t)$ into the energy dissipative law (2.6) as

$$\frac{\partial v_1}{\partial t} = \kappa_1\Delta v_1 + \kappa_1|\nabla v_1|^2 - \frac{\chi_1}{\exp(v_1)}\nabla\cdot(\eta(\rho_1)\nabla c), \tag{3.6}$$

$$\frac{\partial v_2}{\partial t} = \kappa_2\Delta v_2 + \kappa_2|\nabla v_2|^2 - \frac{\chi_2}{\exp(v_2)}\nabla\cdot(\eta(\rho_2)\nabla c). \tag{3.7}$$

$$\rho_1 = \exp(v_1), \quad \rho_2 = \exp(v_2), \tag{3.8}$$

$$\tau\frac{\partial c}{\partial t} = \beta\Delta c - \alpha c + \gamma_1\rho_1 + \gamma_2\rho_2, \tag{3.9}$$

$$\frac{dr}{dt} = -\frac{r}{E(\rho_1, \rho_2, c)} G(\rho_1, \rho_2, c), \tag{3.10}$$

where $G(\rho_1, \rho_2, c) = \int_\Omega \left(\frac{\chi_1}{\gamma_1}\eta(\rho_1)\left(\nabla\frac{\delta E_{tot}}{\delta\rho_1}\right)^2 + \frac{\chi_2}{\gamma_2}\eta(\rho_2)\left(\nabla\frac{\delta E_{tot}}{\delta\rho_2}\right)^2 + \tau\left(\frac{\partial c}{\partial t}\right)^2\right) d\boldsymbol{x} \geq 0$, and the boundary conditions are periodic or

$$\kappa_1\frac{\partial v_1}{\partial \mathbf{n}} - \frac{\chi_1\eta(\rho_1)}{\exp(v_1)}\frac{\partial c}{\partial \mathbf{n}} = 0, \quad \kappa_2\frac{\partial v_2}{\partial \mathbf{n}} - \frac{\chi_2\eta(\rho_2)}{\exp(v_2)}\frac{\partial c}{\partial \mathbf{n}} = 0, \quad \frac{\partial c}{\partial \mathbf{n}} = 0, \quad \text{on } \partial\Omega. \tag{3.11}$$

We construct k-th order fully decoupled and positivity preserving R-GSAV schemes for the above system based on the k-th order implicit-explicit BDF formula as follows.

Scheme 3.1 (k-th order fully decoupled and positivity preserving R-GSAV schemes) Given $(v_1^j, v_2^j, \rho^j, c^j, r^j)$, $j = n, n-1, \ldots, n-k+1$, we find $(v_1^{n+1}, v_2^{n+1}, \rho^{n+1}, c^{n+1}, r^{n+1})$ as follows:

Step 1. Find v_1^{n+1}, v_2^{n+1} by solving the following linear equations with constant coefficients:

$$\begin{aligned}
&\frac{\alpha_k v_1^{n+1} - A_k(v_1^n)}{\delta t} - \kappa_1 \Delta v_1^{n+1} = \kappa_1 |\nabla B_k(v_1^n)|^2 - \frac{\chi_1}{\exp\left(B_k(v_1^n)\right)} \nabla \cdot \left(\eta\left(B_k(\rho_1^n)\right) \nabla B_k(c^n)\right), \\
&\left(\kappa_1 \exp(B_k(v_1^n)) \frac{\partial v_1^{n+1}}{\partial \mathbf{n}} - \chi_1 \eta\left(B_k(\rho_1^n)\right) \frac{\partial B_k(c^n)}{\partial \mathbf{n}}\right) |_{\partial\Omega} = 0,
\end{aligned} \tag{3.12}$$

$$\begin{aligned}
&\frac{\alpha_k v_2^{n+1} - A_k(v_2^n)}{\delta t} - \kappa_2 \Delta v_2^{n+1} = \kappa_2 |\nabla B_k(v_2^n)|^2 - \frac{\chi_2}{\exp\left(B_k(v_2^n)\right)} \nabla \cdot \left(\eta\left(B_k(\rho_2^n)\right) \nabla B_k(c^n)\right), \\
&\left(\kappa_2 \exp(B_k(v_2^n)) \frac{\partial v_2^{n+1}}{\partial \mathbf{n}} - \chi_2 \eta\left(B_k(\rho_1^n)\right) \frac{\partial B_k(c^n)}{\partial \mathbf{n}}\right) |_{\partial\Omega} = 0.
\end{aligned} \tag{3.13}$$

Step 2. Compute the following quantities directly:

$$\bar{\rho_1}^{n+1} = \exp(v_1^{n+1}), \quad \bar{\rho_2}^{n+1} = \exp(v_2^{n+1}), \tag{3.14}$$

$$\lambda_1^{n+1} = \frac{\int_\Omega A_k(\rho_1^n) d\boldsymbol{x}}{\int_\Omega \alpha_k \bar{\rho_1}^{n+1} d\boldsymbol{x}}, \quad \lambda_2^{n+1} = \frac{\int_\Omega A_k(\rho_2^n) d\boldsymbol{x}}{\int_\Omega \alpha_k \bar{\rho_2}^{n+1} d\boldsymbol{x}}, \tag{3.15}$$

$$\rho_1^{n+1} = \lambda_1^{n+1} \bar{\rho}_1^{n+1}, \quad \rho_2^{n+1} = \lambda_2^{n+1} \bar{\rho}_2^{n+1}. \tag{3.16}$$

Step 3. Find c^{n+1} by solving the following linear equations with constant coefficients:

$$\tau \frac{\alpha_k \bar{c}^{n+1} - A_k(\bar{c}^n)}{\delta t} - \beta \Delta \bar{c}^{n+1} + \alpha \bar{c}^{n+1} = \gamma_1 \rho_1^{n+1} + \gamma_2 \rho_2^{n+1}, \quad \frac{\partial \bar{c}^{n+1}}{\partial \mathbf{n}} |_{\partial\Omega} = 0. \tag{3.17}$$

Step 4. Compute the following quantities directly:

$$\frac{\widetilde{r}^{n+1} - r^n}{\delta t} = -\frac{\widetilde{r}^{n+1}}{E(\overline{\rho}_1^{n+1}, \overline{\rho}_2^{n+1}, \overline{c}^{n+1})} G(\overline{\rho}_1^{n+1}, \overline{\rho}_2^{n+1}, \overline{c}^{n+1}), \tag{3.18}$$

$$\xi^{n+1} = \frac{\widetilde{r}^{n+1}}{E(\overline{\rho}_1^{n+1}, \overline{\rho}_2^{n+1}, \overline{c}^{n+1})}, \tag{3.19}$$

$$\eta_k^{n+1} = 1 - \left(1 - \xi^{n+1}\right)^k, \tag{3.20}$$

$$c^{n+1} = \eta_k^{n+1} \overline{c}^{n+1}. \tag{3.21}$$

Step 5. Determine ζ_0^{n+1} (see Theorem 3.1 below) in the admissible set

$$\mathcal{V} = \left\{ \zeta \in [0,1] s.t. \frac{r^{n+1} - \widetilde{r}^{n+1}}{\delta t} = -\gamma^{n+1} G(\rho_1^{n+1}, \rho_2^{n+1}, c^{n+1}) + \frac{\widetilde{r}^{n+1} G(\overline{\rho}_1^{n+1}, \overline{\rho}_2^{n+1}, \overline{c}^{n+1})}{E(\overline{\rho}_1^{n+1}, \overline{\rho}_2^{n+1}, \overline{c}^{n+1})} \right\}, \tag{3.22}$$

with $\gamma^{n+1} \geq 0$ to be determined so that $\mathcal{V}$ is not empty, and update r^{n+1} with

$$r^{n+1} = \zeta_0^{n+1}\tilde{r}^{n+1} + (1-\zeta_0^{n+1})E(\rho_1^{n+1}, \rho_2^{n+1}, c^{n+1}). \tag{3.23}$$

In the above α_k, A_k and B_k $(k = 1, 2, 3)$ are given by:
first-order scheme:

$$\alpha_1 = 1, \quad A_1(v^n) = v^n, \quad B_1(w^n) = w^n;$$

second-order scheme:

$$\alpha_2 = \frac{3}{2}, \quad A_2(v^n) = 2v^n - \frac{1}{2}v^{n-1}, \quad B_2(w^n) = 2w^n - w^{n-1};$$

third-order scheme:

$$\alpha_3 = \frac{11}{6}, \quad A_3(v^n) = 3v^n - \frac{3}{2}v^{n-1} + \frac{1}{3}v^{n-2}, \quad B_3(w^n) = 3w^n - 3w^{n-1} + w^{n-2}.$$

The formula for $k = 4, 5, 6$ can be derived similarly.

Remark 3.2 We note that Scheme 3.1 is fully decoupled and can be solved sequentially. The main computational costs are: (i) Solving v_1^{n+1} from (3.12); (ii) Solving v_2^{n+1} from (3.13); and (iii) Solving c^{n+1} from (3.17). These are all elliptic equations with constant coefficients, which can be solved very efficiently.

We now discuss how to determine ζ_0^{n+1} and γ^{n+1}. Plugging the equation (3.23) into (3.22), we observe that if we choose ζ_0^{n+1} and γ^{n+1} such that

$$\begin{aligned}
&\left(\tilde{r}^{n+1} - E(\rho_1^{n+1}, \rho_2^{n+1}, c^{n+1})\right)\zeta_0^{n+1} \\
&\quad = \tilde{r}^{n+1} - E(\rho_1^{n+1}, \rho_2^{n+1}, c^{n+1}) - \delta t\gamma^{n+1}G(\rho_1^{n+1}, \rho_2^{n+1}, c^{n+1}) \\
&\qquad + \delta t\frac{\tilde{r}^{n+1}G(\overline{\rho}_1^{n+1}, \overline{\rho}_2^{n+1}, \overline{c}^{n+1})}{E(\overline{\rho}_1^{n+1}, \overline{\rho}_2^{n+1}, \overline{c}^{n+1})},
\end{aligned} \tag{3.24}$$

then, $\zeta_0^{n+1} \in \mathcal{V}$.

The choice of ζ_0^{n+1} and γ^{n+1} as well as properties of Scheme 3.1 are summarized in the theorem below.

Theorem 3.1 *We choose ζ_0^{n+1} in (3.23) and γ^{n+1} in (3.22) as follows*:

1. *If* $\tilde{r}^{n+1} = E(\rho_1^{n+1}, \rho_2^{n+1}, c^{n+1})$, *we set* $\zeta_0^{n+1} = 0$ *and* $\gamma^{n+1} = \frac{\tilde{r}^{n+1}G(\overline{\rho}_1^{n+1}, \overline{\rho}_2^{n+1}, \overline{c}^{n+1})}{E(\overline{\rho}_1^{n+1}, \overline{\rho}_2^{n+1}, \overline{c}^{n+1})G(\rho_1^{n+1}, \rho_2^{n+1}, c^{n+1})}$.
2. *If* $\tilde{r}^{n+1} > E(\rho_1^{n+1}, \rho_2^{n+1}, c^{n+1})$, *we set* $\zeta_0^{n+1} = 0$ *and* $\gamma^{n+1} = \frac{\tilde{r}^{n+1} - E(\rho_1^{n+1}, \rho_2^{n+1}, c^{n+1})}{\delta t G(\rho_1^{n+1}, \rho_2^{n+1}, c^{n+1})} + \frac{\tilde{r}^{n+1}G(\overline{\rho}_1^{n+1}, \overline{\rho}_2^{n+1}, \overline{c}^{n+1})}{E(\overline{\rho}_1^{n+1}, \overline{\rho}_2^{n+1}, \overline{c}^{n+1})G(\rho_1^{n+1}, \rho_2^{n+1}, c^{n+1})}$.
3. *If* $\tilde{r}^{n+1} < E(\rho_1^{n+1}, \rho_2^{n+1}, c^{n+1})$ *and* $\tilde{r}^{n+1} - E(\rho_1^{n+1}, \rho_2^{n+1}, c^{n+1}) + \delta t\frac{\tilde{r}^{n+1}G(\overline{\rho}_1^{n+1}, \overline{\rho}_2^{n+1}, \overline{c}^{n+1})}{E(\overline{\rho}_1^{n+1}, \overline{\rho}_2^{n+1}, \overline{c}^{n+1})} \geq 0$, *we set* $\zeta_0^{n+1} = 0$ *and* $\gamma^{n+1} = \frac{\tilde{r}^{n+1} - E(\rho_1^{n+1}, \rho_2^{n+1}, c^{n+1})}{\delta t G(\rho_1^{n+1}, \rho_2^{n+1}, c^{n+1})} + \frac{\tilde{r}^{n+1}G(\overline{\rho}_1^{n+1}, \overline{\rho}_2^{n+1}, \overline{c}^{n+1})}{E(\overline{\rho}_1^{n+1}, \overline{\rho}_2^{n+1}, \overline{c}^{n+1})G(\rho_1^{n+1}, \rho_2^{n+1}, c^{n+1})}$.

4. *If* $\widetilde{r}^{n+1} < E(\rho_1^{n+1}, \rho_2^{n+1}, c^{n+1})$ *and* $\tilde{r}^{n+1} - E(\rho_1^{n+1}, \rho_2^{n+1}, c^{n+1}) + \delta t \frac{\tilde{r}^{n+1} G(\overline{\rho}_1^{n+1}, \overline{\rho}_2^{n+1}, \overline{c}^{n+1})}{E(\overline{\rho}_1^{n+1}, \overline{\rho}_2^{n+1}, \overline{c}^{n+1})} < 0$, *we set* $\zeta_0^{n+1} = 1 - \frac{\delta t \tilde{r}^{n+1} G(\overline{\rho}_1^{n+1}, \overline{\rho}_2^{n+1}, \overline{c}^{n+1})}{E(\overline{\rho}_1^{n+1}, \overline{\rho}_2^{n+1}, \overline{c}^{n+1})(E(\rho_1^{n+1}, \rho_2^{n+1}, c^{n+1}) - \tilde{r}^{n+1})}$ *and* $\gamma^{n+1} = 0$.

Then, (3.24) *is satisfied in all cases above and* $\zeta_0^{n+1} \in \mathcal{V}$. *Besides, given* $\rho_i^j > 0$ *such that*

$$\int_\Omega \rho_i^j d\boldsymbol{x} = \int_\Omega \rho_i^0 d\boldsymbol{x}, \quad i = 1, 2, \quad j = n, n-1, \ldots, n-k+1. \tag{3.25}$$

The Scheme 3.1 *is uniquely solvable and satisfies the following properties unconditionally*:

- *Positivity preserving*: $\rho_i^{n+1} > 0$ $(i = 1, 2)$.
- *Mass conserving*: $\int_\Omega \rho_i^{n+1} d\boldsymbol{x} = \int_\Omega \rho_i^0 d\boldsymbol{x}$ $(i = 1, 2)$.
- *Given* $r^n \geq 0$, *we have* $r^{n+1} \geq 0$, $\xi^{n+1} \geq 0$, *and the Scheme* 3.1 *with the above choice of* ζ_0^{n+1} *and* γ^{n+1} *is unconditionally energy stable in the sense that*

$$r^{n+1} - r^n = -\delta t \gamma^{n+1} G(\rho_1^{n+1}, \rho_2^{n+1}, c^{n+1}) \leq 0. \tag{3.26}$$

Moreover,

$$r^{n+1} \leq E(\rho_1^{n+1}, \rho_2^{n+1}, c^{n+1}), \quad \forall n. \tag{3.27}$$

- *There exists constant* S_k, *such that*

$$E_0(c^n) = \int_\Omega \left(\frac{\beta}{2} |\nabla c^n|^2 + \frac{\alpha}{4} (c^n)^2 \right) d\boldsymbol{x} \leq S_k^2, \quad \forall n. \tag{3.28}$$

Proof From (3.14), we have $\bar{\rho}_i^{n+1} > 0$ $(i = 1, 2)$.

Based on (3.25) and the definition of coefficients α_k and A_k, we have

$$\int_\Omega A_k(\rho_i^n) d\boldsymbol{x} = \alpha_k \int_\Omega \rho_i^0 d\boldsymbol{x}, \quad i = 1, 2. \tag{3.29}$$

Followed by (3.29) and (3.15), we obtain

$$\lambda^{n+1} \int_\Omega \bar{\rho}_i{}^{n+1} d\boldsymbol{x} = \int_\Omega \rho_i^0 d\boldsymbol{x}, \quad i = 1, 2. \tag{3.30}$$

Thanks to $\bar{\rho}_i^{n+1} > 0$, we know that $\lambda_i^{n+1} > 0$. Then (3.16) implies $\rho_i^{n+1} > 0$. Therefore, we derive that $\int_\Omega \rho_i^{n+1} d\boldsymbol{x} = \int_\Omega \rho_i^0 d\boldsymbol{x}$ $(i = 1, 2)$.

Given $r^n \geq 0$, it follows from (3.18) that

$$\widetilde{r}^{n+1} = \frac{r^n}{1 + \delta t \frac{G(\overline{\rho}_1^{n+1}, \overline{\rho}_2^{n+1}, \overline{c}^{n+1})}{E(\overline{\rho}_1^{n+1}, \overline{\rho}_2^{n+1}, \overline{c}^{n+1})}} \geq 0 \tag{3.31}$$

since that $G(\overline{\rho}_1^{n+1}, \overline{\rho}_2^{n+1}, \overline{c}^{n+1}) \geq 0$ and $E(\overline{\rho}_1^{n+1}, \overline{\rho}_2^{n+1}, \overline{c}^{n+1}) > 0$. Then (3.19) implies $\xi^{n+1} \geq 0$ and (3.23) implies $r^{n+1} \geq 0$. Additionally, we get (3.26) by combining (3.18) and (3.22).

In Cases 1-3, we have $\zeta_0^{n+1} = 0$ so $r^{n+1} = E(\rho_1^{n+1}, \rho_2^{n+1}, c^{n+1})$. In Case 4, due to $\zeta_0^{n+1} = 1 - \frac{\delta t \tilde{r}^{n+1} G(\overline{\rho}_1^{n+1}, \overline{\rho}_2^{n+1}, \overline{c}^{n+1})}{E(\overline{\rho}_1^{n+1}, \overline{\rho}_2^{n+1}, \overline{c}^{n+1})(E(\rho_1^{n+1}, \rho_2^{n+1}, c^{n+1}) - \tilde{r}^{n+1})} \in [0, 1]$ and $\widetilde{r}^{n+1} < E(\rho_1^{n+1}, \rho_2^{n+1}, c^{n+1})$, we know that $r^{n+1} \leq E(\rho_1^{n+1}, \rho_2^{n+1}, c^{n+1})$ from (3.23).

We denote $S_0 := r^0 = E(\rho_1(\cdot,0), \rho_2(\cdot,0), c(\cdot,0))$ and have $\widetilde{r}^{n+1} \le S_0$ $(\forall n)$ from (3.26) and (3.31). As we stated before that $E_1(\rho_1, \rho_2, c) + C_0 \ge 1$ for all ρ_1, ρ_2 and c, we derive from (3.19) that

$$| \xi^{n+1} | = \frac{\widetilde{r}^{n+1}}{E_{tot}(\overline{\rho}_1^{n+1}, \overline{\rho}_2^{n+1}, \overline{c}^{n+1}) + C_0} \le \frac{S_0}{E_0(\overline{c}^{n+1}) + 1}. \tag{3.32}$$

For $\eta_k^{n+1} = 1 - \left(1 - \xi^{n+1}\right)^k$, there exists a polynomial P_{k-1} of $k-1$ and a constant $S_k > 0$ such that

$$| \eta_k^{n+1} | = | \xi^{n+1} P_{k-1}(\xi^{n+1}) | \le \frac{S_k}{E_0(\overline{c}^{n+1}) + 1}. \tag{3.33}$$

Indeed, $\sqrt{A} \le A + 1$ for all $A \ge 0$. Therefore, we derive from (3.20) that

$$\sqrt{E_0(c^{n+1})} = | \eta_k^{n+1} | \sqrt{E_0(\overline{c}^{n+1})} \le S_k,$$

That is,

$$E_0(c^n) = \int_\Omega \left(\frac{\beta}{2} |\nabla c^n|^2 + \frac{\alpha}{4} (c^n)^2 \right) d\boldsymbol{x} \le S_k^2, \quad \forall n.$$

The proof is complete. □

Remark 3.3 Note that in most cases, we can choose $\zeta_0^{n+1} = 0$ such that $r^{n+1} = E(\rho^{n+1}, c^{n+1}, \boldsymbol{u}^{n+1})$ holds. In these cases, we can derive from (3.26) and (3.27) that

$$E(\rho_1^{n+1}, \rho_2^{n+1}, c^{n+1}) = r^{n+1} \le r^n \le E(\rho_1^n, \rho_2^n, c^n),$$

i.e., the original energy is also dissipative when $\zeta_0^{n+1} = 0$.

We observe that the above result also applies to fully discretized versions of Scheme 3.1 with Galerkin-type spatial discretizations with consistent discrete integration by parts.

4 Numerical Simulations and Discussions

We start with verifying the accuracy of fully decoupled R-GSAV schemes for the two-species KS model (1.1)-(1.3). Then, we conduct a series of numerical experiments to investigate blow-up of the model in 3D domains. We first validate the blow-up theoretical results for the model in parabolic-elliptic form [2] and in parabolic-parabolic form [28], respectively, and then explore blow-up with non-radial conditions for the parabolic-parabolic model, which lacks theoretical support. Finally, we modify the classical two-species KS model to eliminate blow-up and present simulations of some interesting chemotaxis phenomena.

For the sake of simplicity, we only consider the periodic boundary conditions in this section, and use the Fourier spectral method for which our schemes lead to diagonal systems at each time step. So they are very efficient and spectrally accurate in space. In all the numerical examples presented below, essential properties of the two-species KS model are preserved, namely, the minimum of ρ_i $(i = 1, 2)$ remains to be non-negative, the mass of ρ_i $(i = 1, 2)$ is conserved, and the total energy is dissipative.

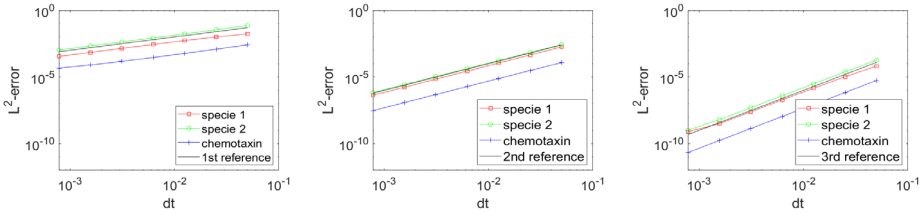

(a) first-order scheme (b) second-order scheme (c) third-order scheme

Fig. 1 The convergence in L^2-norm for the two-species KS model

4.1 Accuracy Test

We test the accuracy of Scheme 3.1 ($k = 1, 2, 3$) for the two-species KS system (1.1)-(1.3) in $\Omega = (0, 2)^3$. We set all coefficients in (1.1)-(1.3) equal to one, and consider the exact solutions:

$$\begin{cases} \rho_1 = \sin(\pi x)\sin(\pi y)\sin(\pi z)\sin(t) + 1.1, \\ \rho_2 = \cos(\pi x)\cos(\pi y)\cos(\pi z)\sin(t) + 1.1, \\ c = \sin(\pi x)\sin(\pi y)\sin(\pi z)\sin(t) + 1.1, \end{cases} \tag{4.1}$$

with a corresponding external forcing term on the right hand side. The initial data are determined by exact solutions. We apply the Fourier-spectral method in space with modes $N = 40$ in each spatial direction, so that the spatial discretization error is negligible with respect to the time discretization error. The expected convergence rates in the L^2-norm at $T = 1$ are shown in Fig. 1.

4.2 Blow-up of the Parabolic-Elliptic Model

Next, we use the third order Scheme 3.1 ($k = 3$) to simulate the two-species KS model in parabolic-elliptic form with $\tau = \alpha = 0$ and $\beta = \gamma_1 = \gamma_2 = 1$ in a bounded domain $\Omega = (-1, 1)^3$. We perform a series of numerical simulations to verify the blow-up condition (2.7) and investigate effects of parameters on the blow-up.

Example 1 *Blow-up with $M_1 = M_2 < 8\pi$.* We set $\kappa_1 = \kappa_2 = \chi_1 = \chi_2 = 1$ for the parabolic-elliptic model and initial data

$$\rho_{10} = \rho_{20} = 35\exp\left(-4\left(x^2 + y^2 + z^2\right)\right). \tag{4.2}$$

Note that the initial masses of the two species ρ_1 and ρ_2 are $M_1 = M_2 \approx 24.02 < 8\pi$, according to (2.7) we have $L \approx 0.3462$ and $R \approx 0.4506$. Hence, the blow-up condition (2.7) is satisfied. We use Fourier modes $N = 200$ in each direction, and set the time step to $dt = 1e-4$. The results are plotted in Fig. 2. In Fig. 2 (a), we observe that the maxima of ρ_1 and ρ_2 increase rapidly as their orders of magnitude increase from 1 to 4, and they blow up simultaneously in finite time. On the other hand, the minima of ρ_1 and ρ_2 are always non-negative in Fig. 2 (b), which indicates the positivity of population densities is preserved. Figure 2 (c) and (d) demonstrate that the mass of population density is conserved, and the total energy is dissipative in the whole process.

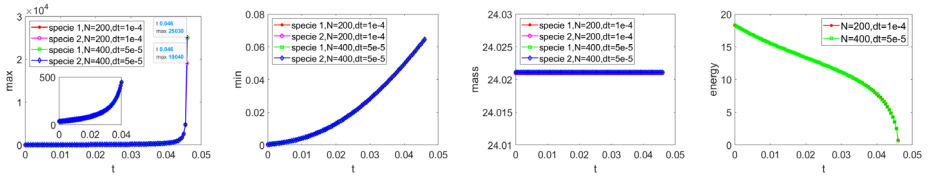

(a) max ρ_i (b) min ρ_i (c) mass (d) total energy

Fig. 2 Example 1: Evolutions of max ρ_i, min ρ_i, mass of ρ_i $(i = 1, 2)$ and total energy E_{tot} with $N = 200$, $dt = 1e-4$ and $N = 400$, $dt = 5e-5$

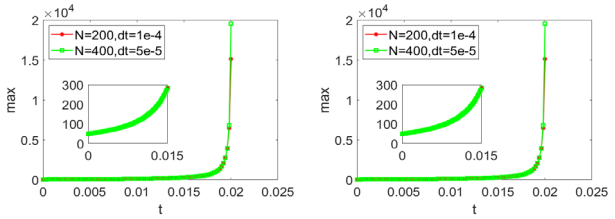

(a) max ρ_1 (b) max ρ_2

Fig. 3 Example 2: Evolutions of max ρ_i $(i = 1, 2)$ with $N = 200$, $dt = 1e-4$ and $N = 400$, $dt = 5e-5$

To further verify the blow-up, a mesh refinement study with $N = 400$ and $dt = 5e-5$ is performed and the results are also plotted in Fig. 2. Compared with $N = 200$ and $dt = 1e-4$, we observe a slight change in the maxima of ρ_i $(i = 1, 2)$, but the minima, mass of ρ_i $(i = 1, 2)$, and the total energy are almost unchanged compared. It also indicates that ρ_i $(i = 1, 2)$ had blown up by the time $t = 0.046$.

Example 2 *Blow-up with* $M_1 = M_2 > 8\pi$. We keep $\kappa_1 = \kappa_2 = \chi_1 = \chi_2 = 1$ but change the initial data to

$$\rho_{10} = \rho_{20} = 50 \exp\left(-4\left(x^2 + y^2 + z^2\right)\right). \tag{4.3}$$

Now the initial masses of two species ρ_1 and ρ_2 are $M_1 = M_2 \approx 34.32 > 8\pi$, and correspondingly we have $L \approx 0.3462 < R \approx 0.6436$ which also satisfies the blow-up condition (2.7). We use two sets of meshes, $(N = 200, dt = 1e-4)$ and $(N = 400, dt = 5e-5)$, and plot the results in Fig. 3. We find that ρ_1 and ρ_2 blow up by the time $t = 0.02$.

We also plot several snapshots of the density ρ_1 in Fig. 4. Snapshots of ρ_2 are omitted as they are essentially the same as those of ρ_1. From the distribution of ρ_1 on the plane $y = 0$, we observe that the density accumulates toward the regional center, and the density at the center increases over time. In order to present the distribution of ρ_1 in the 3D space, we plot the iso-surface of ρ_1 with iso-value $R_{1t}/2$, where $R_{1t} = \rho_{1\max}(t) + \rho_{1\min}(t)$. By the time $t = 0.02$, almost all populations are concentrated at the center of the region, as the iso-surface of $R_{1t}/2$ reduces to one point.

Example 3 *Faster blow-up with a larger chemotaxis sensitivity coefficient.* We keep $\kappa_1 = \kappa_2 = \chi_1 = 1$ and initial data (4.3), but increase the sensitivity coefficient χ_2 to 10. In this case, the corresponding $L \approx 0.2567$ is still less than $R \approx 0.3701$, satisfying the blow-up condition (2.7). We still use two sets of meshes, $(N = 200, dt = 1e-5)$ and $(N = 400,$

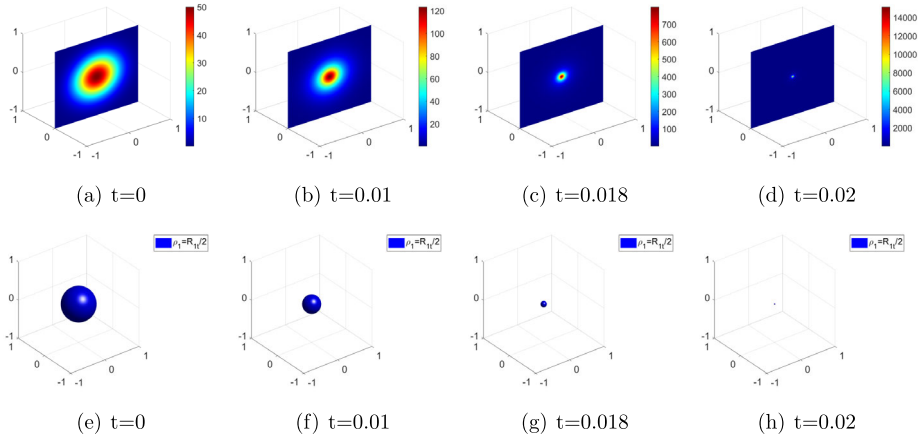

Fig. 4 Example 2: Snapshots of the density ρ_1 (the slice on Y-direction (top) and the isosurface (bottom))

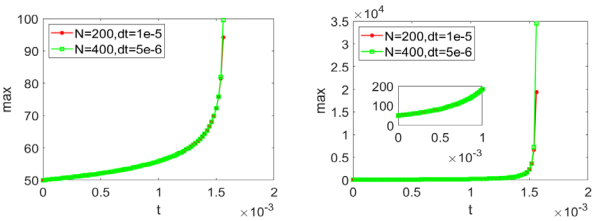

Fig. 5 Example 3: Evolutions of max ρ_i $(i = 1, 2)$ with $N = 200$, $dt = 1e-5$ and $N = 400$, $dt = 5e-6$

$dt = 5e-6$), and plot the results in Fig. 5. We observe from Fig. 5 that the maximum of ρ_2 increases much faster than that of ρ_1, and by the time $t = 0.00156$, ρ_2 has already blown up. This example reveals that ρ_2 with larger chemotaxis sensitivity coefficient χ_2 blows up faster than ρ_1. Besides, compared with Example 2, it blows up in a shorter time. As s result, the larger $\chi_i (i = 1, 2)$ is, the faster blow-up occurs.

Example 4 *Faster blow-up with larger initial mass of ρ_i $(i = 1, 2)$.* We keep $\kappa_1 = \kappa_2 = \chi_1 = \chi_2 = 1$, but change the initial data to

$$\rho_{10} = 50 \exp\left(-4\left(x^2 + y^2 + z^2\right)\right), \quad \rho_{20} = 500 \exp\left(-4\left(x^2 + y^2 + z^2\right)\right). \tag{4.4}$$

In this case, we still have $L \approx 0.3527 < R \approx 3.5400$. We use the same two sets of meshes as in the last example, and plot the results in Fig. 6. The maximum of ρ_2 increases faster than that of ρ_1, and that ρ_1 and ρ_2 blow up by the time $t = 0.00212$. Compared with Example 2, the blow-up happens in a shorter time, which indicates that increasing initial mass of ρ_2 leads to faster blow-up.

Example 5 *Faster blow-up with smaller diffusion coefficient of ρ_i $(i = 1, 2)$.* We keep $\kappa_1 = \chi_1 = \chi_2 = 1$ and initial data (4.3), but decrease the diffusion coefficient κ_2 to 0.1. In this case, $L \approx 0.3462 < R \approx 1.1703$ which still satisfied the blow-up condition (2.7). Figure 7

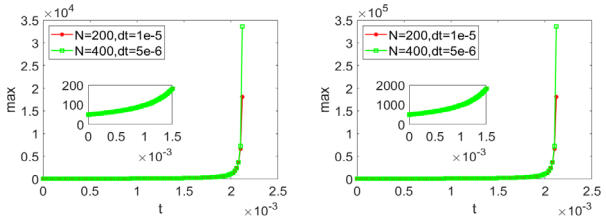

Fig. 6 Example 4: Evolutions of max ρ_i $(i = 1, 2)$ with $N = 200$, $dt = 1e-5$ and $N = 400$, $dt = 5e-6$

(a) max ρ_1 (b) max ρ_2

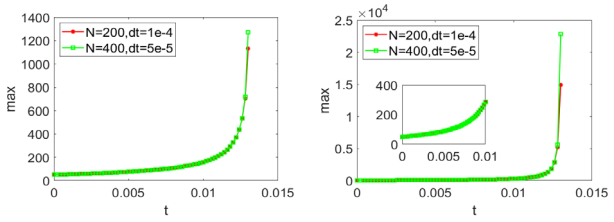

Fig. 7 Example 5: Evolutions of max ρ_i $(i = 1, 2)$ with $N = 200$, $dt = 1e-4$ and $N = 400$, $dt = 5e-5$

(a) max ρ_1 (b) max ρ_2

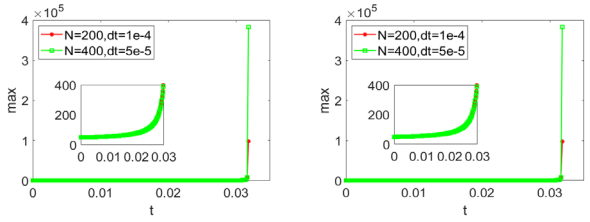

Fig. 8 Example 6: Evolutions of max ρ_i $(i = 1, 2)$ with $N = 200$, $dt = 1e-4$ and $N = 400$, $dt = 5e-5$

(a) max ρ_1 (b) max ρ_2

shows that the magnitude order of ρ_1 increases from 1 to 3, the magnitude order of ρ_2 increases from 1 to 4, and by the time $t = 0.013$ ρ_1 and ρ_2 have already blown up. Besides, ρ_2 with smaller diffusion coefficient κ_2 blows up faster than ρ_1. Moreover, compared with Example 2, the blow-up speed in this case is significantly increased.

Example 6 *Blow-up at the corner.* We set $\kappa_1 = \kappa_2 = \chi_1 = \chi_2 = 1$ and the initial data

$$\rho_{10} = \rho_{20} = 50 \exp\left(-\frac{1}{25}\left(\left(x-\frac{1}{2}\right)^2 + \left(y-\frac{1}{2}\right)^2 + \left(z-\frac{1}{2}\right)^2\right)\right), \tag{4.5}$$

where $L_1 \approx 3.1494 < R_1 \approx 6.9983$ satisfies the blow-up condition (2.7). The results are presented in Fig. 8 and Fig. 9. We find in Fig. 8 that maxima of ρ_1 and ρ_2 keep increasing in the same way, their magnitude orders increase from 1 to 5, and they have already blown up by the time $t = 0.0318$. We observe from Fig. 9 (a)-(d) that the density ρ_1 accumulates toward the top right corner, and the density at the corner increases over time. Finally, almost all the density is concentrated at the corner of the region, so that the iso-surface of $R_{1t}/2$ at $t = 0.0318$ approximates a point, see Fig. 9 (h).

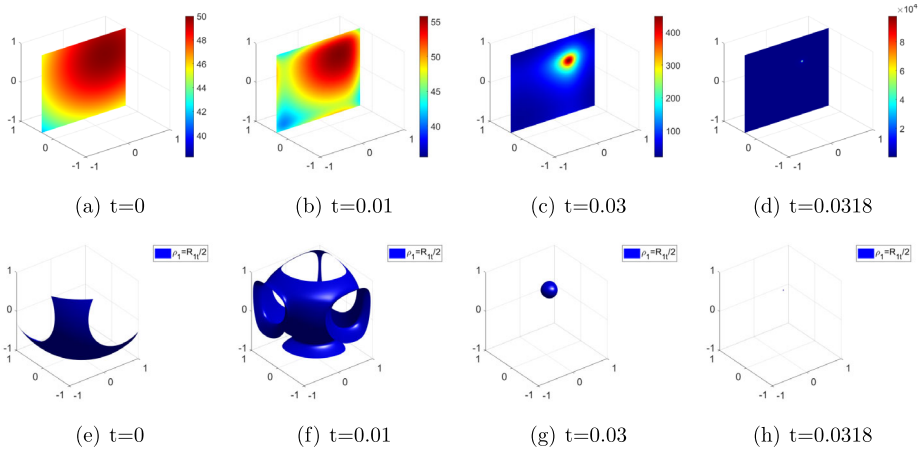

(a) t=0 (b) t=0.01 (c) t=0.03 (d) t=0.0318

(e) t=0 (f) t=0.01 (g) t=0.03 (h) t=0.0318

Fig. 9 Example 6: Snapshots of the density ρ_1 (the slice on Y-direction (top) and the isosurface (bottom))

Fig. 10 Example 7: Evolutions of max ρ_i $(i = 1, 2)$ with $N = 200$, $dt = 1e-4$ and $N = 400$, $dt = 5e-5$

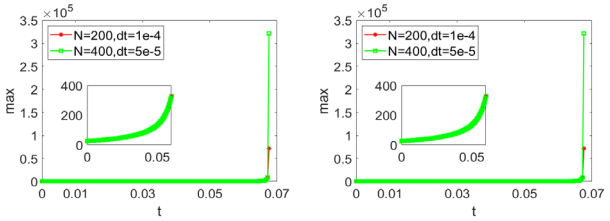

(a) max ρ_1 (b) max ρ_2

Example 7 *Blow-up with non-radial initial data.* We set non-radial initial data

$$\begin{cases} \rho_{10} = 25 \exp\left(-4\left(x^2/16 + y^2 + z^2\right)\right), \\ \rho_{20} = 25 \exp\left(-4\left(x^2 + y^2/16 + z^2\right)\right), \end{cases} \tag{4.6}$$

and keep $\kappa_1 = \kappa_2 = \chi_1 = \chi_2 = 1$. Here $L \approx 0.4760 < R \approx 0.6732$ still meets the blow-up condition (2.7). We observe in Fig. 10 that the magnitude orders of ρ_1 and ρ_2 both increase from 1 to 5, and have already blown up by the time $t = 0.0676$. We also plot several snapshots of the density ρ_1 and ρ_2 in Fig. 11 and Fig. 12, respectively. For the distribution of ρ_1 on the plane $y = 0$, the density ρ_1 accumulates toward the regional center, and the density at the center increases over time. The evolution of distribution of ρ_2 is similar to that of ρ_1 after rotating 90 degrees.

4.3 Blow-up of the Parabolic-Parabolic Model

Now we apply the third order Scheme 3.1 ($k = 3$) to deal with the two-species KS model in parabolic-parabolic form with $\tau = \kappa_1 = \kappa_2 = \beta = 1$ in $\Omega = (-1, 1)^3$.

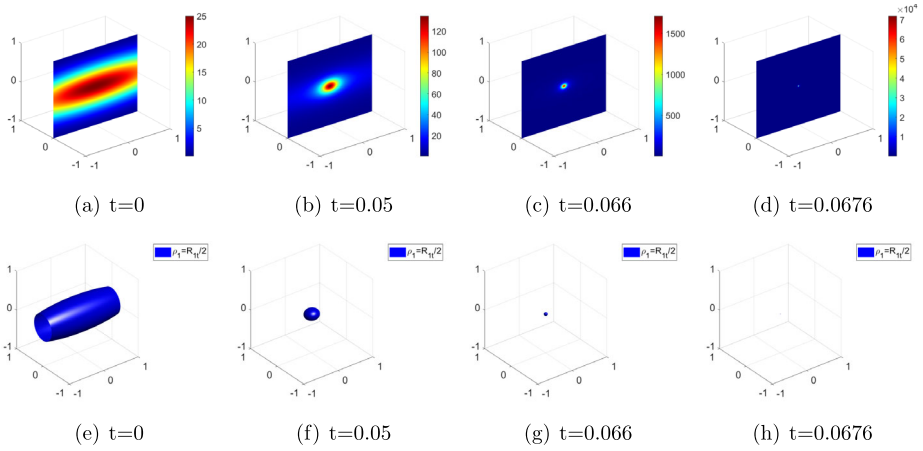

(a) t=0 (b) t=0.05 (c) t=0.066 (d) t=0.0676

(e) t=0 (f) t=0.05 (g) t=0.066 (h) t=0.0676

Fig. 11 Example 7: Snapshots of the density ρ_1 (the slice on Y-direction (top) and the isosurface (bottom))

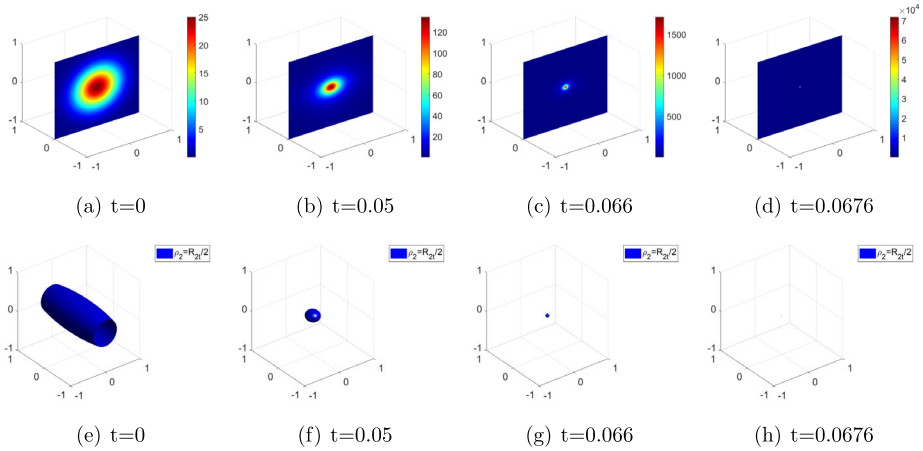

(a) t=0 (b) t=0.05 (c) t=0.066 (d) t=0.0676

(e) t=0 (f) t=0.05 (g) t=0.066 (h) t=0.0676

Fig. 12 Example 7: Snapshots and of the cell density ρ_2 (the slice on Y-direction (top) and the isosurface (bottom))

Example 8 *Blow-up with* $M_1 = M_2 < 8\pi$. We set $\kappa_1 = \kappa_2 = \chi_2 = 1$, $\chi_1 = 10$, $\alpha = 0.001$ and initial data

$$\rho_{10} = \rho_{20} = 35 \exp\left(-4\left(x^2 + y^2 + z^2\right)\right), \quad c_0 = 1, \tag{4.7}$$

where the initial masses of two species population density are $M_1 = M_2 \approx 24.02 < 8\pi$. We observe in Fig. 13 that ρ_1 and ρ_2 have already blown up by the time $t = 0.0186$. Figure 14 shows that the computational results maintain essential physical properties.

Example 9 *Blow-up with* $M_1 = M_2 > 8\pi$. We set $\kappa_1 = \kappa_2 = \chi_1 = \chi_2 = \alpha = 1$ and initial data

$$\rho_{10} = \rho_{20} = 50 \exp\left(-4\left(x^2 + y^2 + z^2\right)\right), \quad c_0 = 1, \tag{4.8}$$

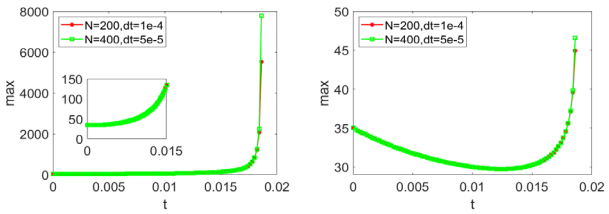

(a) max ρ_1 (b) max ρ_2

Fig. 13 Example 8: Evolutions of max ρ_i $(i = 1, 2)$ with $N = 200$, $dt = 1e-4$ and $N = 400$, $dt = 5e-5$

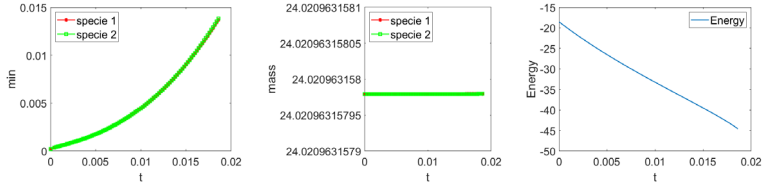

(a) min ρ_i (b) mass (c) total energy

Fig. 14 Example 8: Evolutions of min ρ_i, mass of ρ_i, and total energy E_{tot} $(i = 1, 2)$

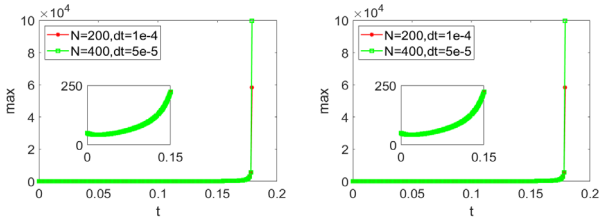

(a) max ρ_1 (b) max ρ_2

Fig. 15 Example 9: Evolutions of max ρ_i $(i = 1, 2)$ with $N = 200$, $dt = 1e-4$ and $N = 400$, $dt = 5e-5$

where the initial masses of two species population density are $M_1 = M_2 \approx 34.32 > 8\pi$. It is clear from Fig. 15 that the maxima of ρ_1 and ρ_2 keep increasing, and they blow up simultaneously at about $t = 0.164$.

Example 10 *Blow-up with non-radial initial data.* We set $\kappa_1 = \kappa_2 = \chi_1 = \chi_2 = 1, \alpha = 0.001$, and take non-radial initial data

$$\rho_{10} = 25\exp\left(-4\left(x^2/16 + y^2 + z^2\right)\right), \quad \rho_{20} = 25\exp\left(-4\left(x^2 + y^2/16 + z^2\right)\right), \quad c_0 = 0. \tag{4.9}$$

Evolutions of max ρ_i $(i = 1, 2)$ with different space-time steps are plotted in Fig. 16, which shows that ρ_1 and ρ_2 blow up simultaneously.

4.4 Prevention of Blow-up with Modified Models

We show in this subsection that the blow-up in parabolic-elliptic form and parabolic-parabolic form can be prevented by modifying the concentration-dependent mobility $\eta(\rho_i) = \rho_i$ to $\eta(\rho_i) = \frac{\rho_i}{1+\epsilon\rho_i}$ and $\eta(\rho_i) = \rho_i(1 - \frac{\rho_i}{S})$ $(i = 1, 2)$.

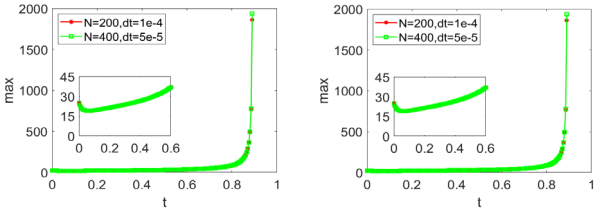

(a) max ρ_1 (b) max ρ_2

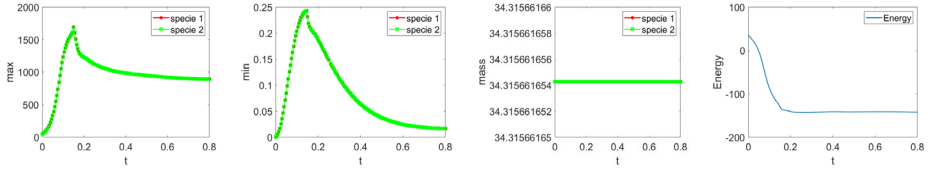

(a) max ρ_i (b) min ρ_i (c) mass (d) total energy

Fig. 16 Example 10: Evolutions of max ρ_i $(i = 1, 2)$ with $N = 200$, $dt = 1e - 4$ and $N = 400$, $dt = 5e - 5$

Fig. 17 Example 11: Evolutions of max ρ_i, min ρ_i, mass of ρ_i, and total energy E_{tot} $(i = 1, 2)$

The examples below are calculated by the third order Scheme 3.1 ($k = 3$) with $N = 200$ and $dt = 1e - 4$ in a bounded domain $\Omega = (-1, 1)^3$. For simplicity, all coefficients are fixed as one. The initial population density is $\rho_{10} = \rho_{20} = 50 \exp\left(-4\left(x^2 + y^2 + z^2\right)\right)$. Note that in parabolic-parabolic form the initial concentration of chemoattractant is $c_0 = 0$.

Example 11 *The modified parabolic-elliptic model with* $\eta(\rho_i) = \frac{\rho_i}{1+\epsilon\rho_i}$ $(i = 1, 2)$ *and* $\epsilon = 0.01$. Fig. 17 shows that the maximum of ρ_i $(i = 1, 2)$ increases until about $t = 0.15$, then decreases until it reaches a steady state. We also observe that the minimum of ρ_i is non-negative, the mass of ρ_i $(i = 1, 2)$ is conserved, the total energy is dissipative all the time. The distributions of ρ_1 on the plane $y = 0$ and the iso-surfaces of ρ_1 at different time are presented in Fig. 18. We observe that the density gathers towards the center until about $t = 0.15$, then diffuses outward until the steady state is reached.

Example 12 *The modified parabolic-elliptic model with* $\eta(\rho_i) = \rho_i(1 - \frac{\rho_i}{S})$ *and* $S = 100$. In this case, we see from Fig. 19 that the maximum of ρ_i $(i = 1, 2)$ increases until it reaches the saturation concentration $S = 100$. Figure 20 indicates the density gathers towards the center until the saturation is reached.

Example 13 *The modified parabolic-parabolic model with* $\eta(\rho_i) = \frac{\rho_i}{1+\epsilon\rho_i}$ $(i = 1, 2)$ *and* $\epsilon = 0.01$. Similar to Example 11, Fig. 21 shows that the maximum of ρ_i $(i = 1, 2)$ first increases then decreases until it reaches the steady state.

Example 14 *The modified parabolic-parabolic model with* $\eta(\rho_i) = \rho_i(1 - \frac{\rho_i}{S})$ *and* $S = 100$. We observe from Fig. 22 that the behaviors are quite different from Example 12 which has the same $\eta(\rho_i)$. More precisely, the maximum of ρ_i $(i = 1, 2)$ increases for a very short time then decreases until it reaches the steady state.

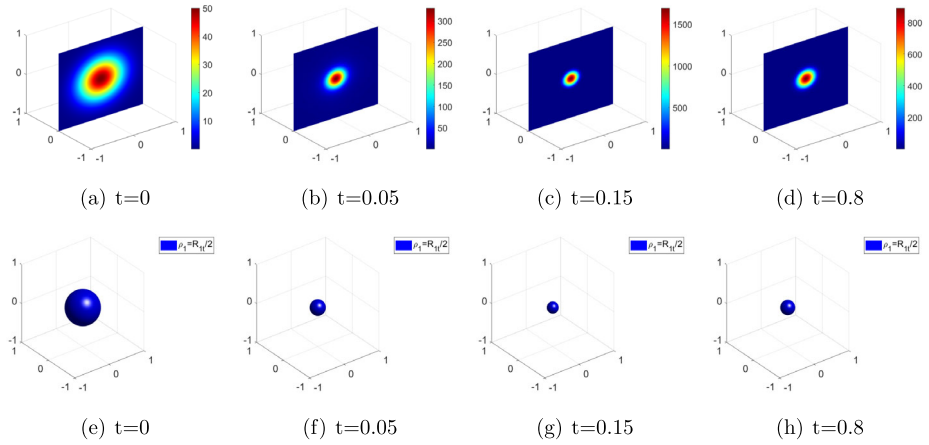

(a) t=0 (b) t=0.05 (c) t=0.15 (d) t=0.8

(e) t=0 (f) t=0.05 (g) t=0.15 (h) t=0.8

Fig. 18 Example 11: Snapshots and of the cell density ρ_1 (the slice on Y-direction (top) and the iso-surface (bottom))

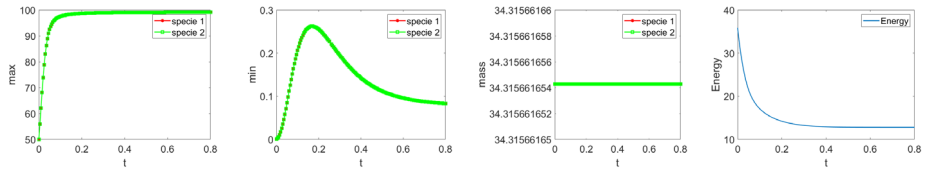

(a) max ρ_i (b) min ρ_i (c) mass (d) total energy

Fig. 19 Example 12: Evolutions of max ρ_i, min ρ_i, mass of ρ_i, and total energy E_{tot} $(i = 1, 2)$

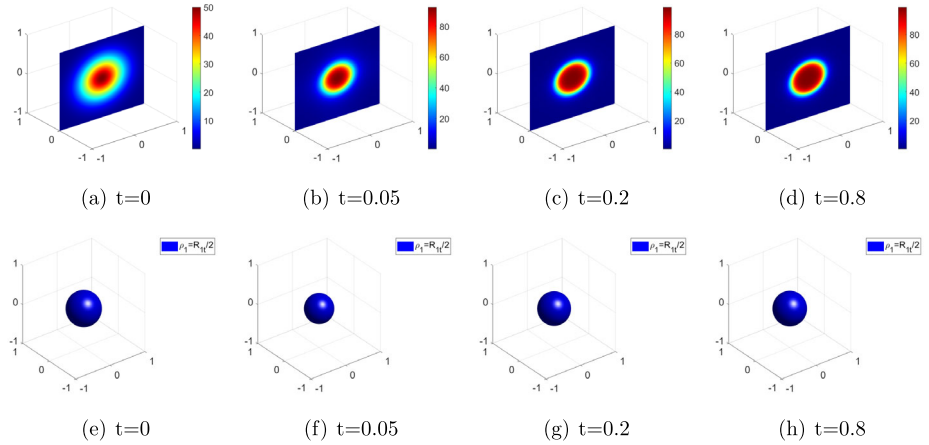

(a) t=0 (b) t=0.05 (c) t=0.2 (d) t=0.8

(e) t=0 (f) t=0.05 (g) t=0.2 (h) t=0.8

Fig. 20 Example 12: Snapshots of the density ρ_1 (the slice on Y-direction (top) and the iso-surface (bottom))

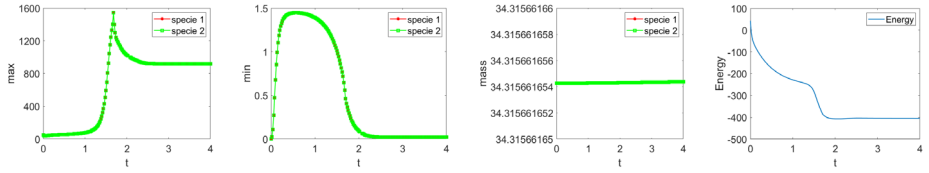

(a) max ρ_i (b) min ρ_i (c) mass (d) total energy

Fig. 21 Example 13: Evolutions of max ρ_i, min ρ_i, mass of ρ_i, and total energy E_{tot} $(i = 1, 2)$

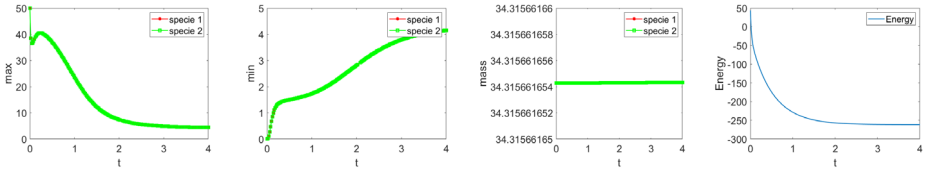

(a) max ρ_i (b) min ρ_i (c) mass (d) total energy

Fig. 22 Example 14: Evolutions of max ρ_i, min ρ_i, mass of ρ_i, and total energy E_{tot} $(i = 1, 2)$

4.5 Chemotaxis Phenomena of the Modified Models

We revealed above that the modified models can prevent blow-up. Next, we show that the modified two-species KS models with $\eta(\rho_i) = \frac{\rho_i}{1+\epsilon\rho_i}$ $(i = 1, 2)$ and $\epsilon = 0.01$ lead to similar chemotaxis phenomena, as the one-species models in [22, 32].

Example 15 *Aggregation phenomenon.* We consider the domain $\Omega = (0, 5)^3$ and the initial conditions

$$\rho_{10} = \rho_{20} = 0.9 + 0.2 * \text{rand}, \quad c_0 = 0. \tag{4.10}$$

We set $\chi_1 = 2$, $\chi_2 = 20$, $\beta = 0.5$, and other coefficients as one, and use the third order Scheme 3.1 ($k = 3$) with $N = 200$ and $dt = 1e - 5$. Snapshots of ρ_1, ρ_2 and c at different time are presented in Fig. 23. They reveal that the aggregating behavior of species, that is, single colonies of species merge together to form one larger colony. Moreover, distributions of two species are both consistent with that of the chemoattractant, which indicates that species gravitate to places with high concentrations of the chemoattractant.

Example 16 *Pattern formation.* We set $\Omega = (-3, 3)^3$, and the initial data

$$\rho_{10} = \rho_{20} = \begin{cases} 1 + \text{rand}, & x^2 + y^2 + z^2 < 3, \\ 1, & \text{else}, \end{cases} \quad c_0 = \frac{1}{32}, \tag{4.11}$$

and $\kappa_1 = \kappa_2 = 0.05$, $\chi_1 = 1$, $\chi_2 = 6$, $\alpha = 16$ with other parameters all equal to one. The third order Scheme 3.1 ($k = 3$) with $N = 200$ and $dt = 1e - 5$ is used. Since the distributions of ρ_1, ρ_2 and c are radial, we draw their slices on the plane $y = 0, -1.5, -3$ at different time in Fig. 24. At first, the two species are scattered in the set area. Over time, they are clustered near the ring pattern, which is similar to the pattern formed by motile cells of Escherichia coli in [4]. Throughout the process, high concentration distributions of the two species are consistent with that of the chemoattractant.

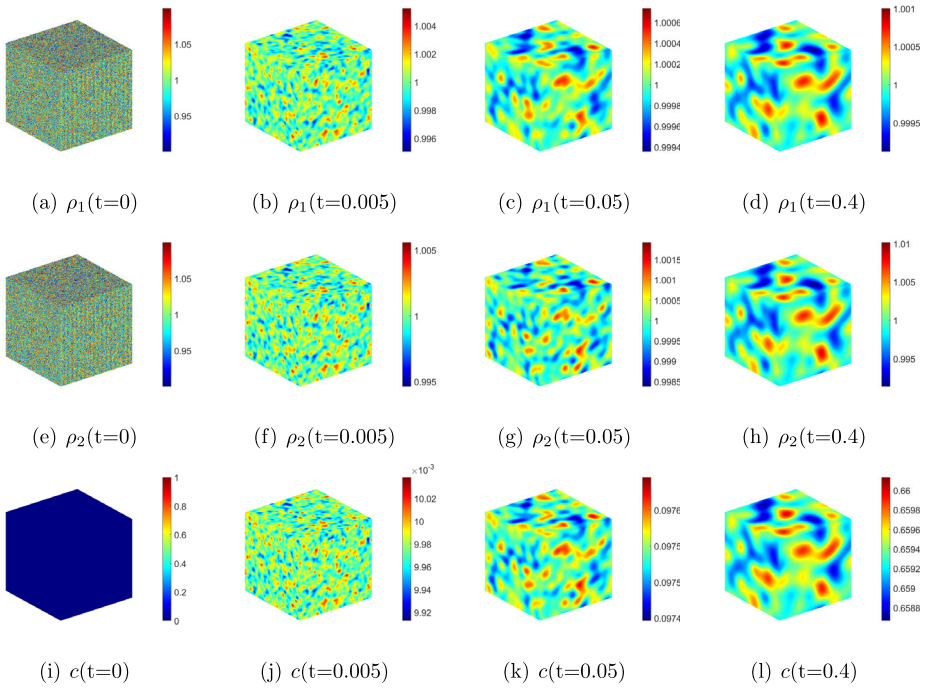

(a) ρ_1(t=0) (b) ρ_1(t=0.005) (c) ρ_1(t=0.05) (d) ρ_1(t=0.4)

(e) ρ_2(t=0) (f) ρ_2(t=0.005) (g) ρ_2(t=0.05) (h) ρ_2(t=0.4)

(i) c(t=0) (j) c(t=0.005) (k) c(t=0.05) (l) c(t=0.4)

Fig. 23 Example 15: Snapshots of ρ_1 (top), ρ_2 (middle) and c (bottom)

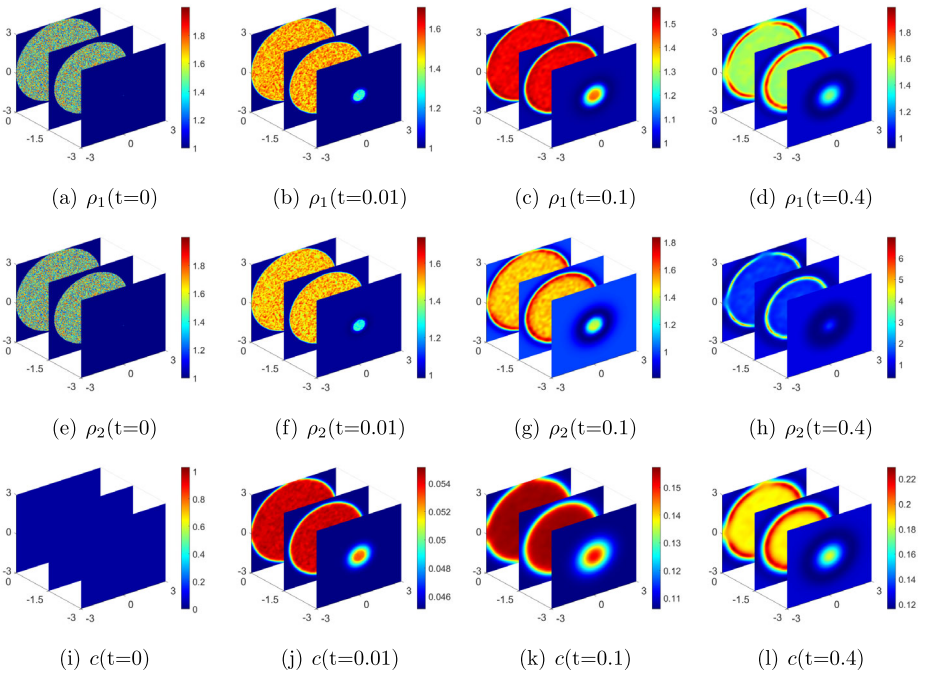

(a) ρ_1(t=0) (b) ρ_1(t=0.01) (c) ρ_1(t=0.1) (d) ρ_1(t=0.4)

(e) ρ_2(t=0) (f) ρ_2(t=0.01) (g) ρ_2(t=0.1) (h) ρ_2(t=0.4)

(i) c(t=0) (j) c(t=0.01) (k) c(t=0.1) (l) c(t=0.4)

Fig. 24 Example 16: Snapshots of ρ_1 (top), ρ_2 (middle) and c (bottom)

5 Conclusions

We developed a class of efficient schemes for the two-species KS model (1.1)-(1.5) by combining a function transform which preserves bound/positivity, and the relaxed generalized SAV approach which is unconditionally energy stable with a modified energy. The schemes are fully decoupled, can be high-order, and only require solving decoupled linear equations with constant coefficients at each time step and can be used with any consistent Galerkin type spatial discretization. They also preserve bound/positivity, mass conservation and energy dissipation at the discrete level.

We performed a large number of numerical experiments using the new schemes with a Fourier-spectral method in space to investigate blow-up phenomena of the two-species KS models in 3D. The main findings are as follows:

- For the two-species KS model in parabolic-elliptic form, ρ_1 and ρ_2 blow up if the initial data satisfy the inequality (2.7), consistent with the theoretical results described in [2], and the blow-up can be accelerated by increasing the chemotaxis sensitivity coefficient χ_i, increasing the initial mass M_i, or decreasing the diffusion coefficient κ_i $(i = 1, 2)$.
- For the two-species KS model in parabolic-parabolic form, regardless of whether the initial mass M_i $(i = 1, 2)$ is larger than 8π, there exists radial initial data that lead to blow-up in finite time, consistent with the theoretical results described in [28]; there existed also radial initial data that lead to blow-up in finite time.
- The blow-up of the two-species KS model, whether in parabolic-elliptic form or parabolic-parabolic form, can be prevented by modifying the concentration-dependent mobility $\eta(\rho_i) = \rho_i$ to $\eta(\rho_i) = \frac{\rho_i}{1+\epsilon\rho_i}$ $(\epsilon > 0)$ or $\eta(\rho_i) = \rho_i(1 - \frac{\rho_i}{S})$ $(S > 0)$ $(i = 1, 2)$; and the modified models lead to similar chemotaxis phenomena, such as the aggregation phenomenon and pattern formation, as the one-species models in [22, 32].

Funding This work is supported in part by NSFC grant 12371409.

Declarations

Competing Interests The authors declare no competing interests.

References

1. Arumugam, G., Tyagi, J.: Keller-Segel Chemotaxis models: a review. Acta Appl. Math. **171**(1), 1–82 (2021)
2. Biler, P., Espejo, E.F., Guerra, I.: Blowup in higher dimensional two species chemotactic models. Commun. Pure Appl. Anal. **12**(1), 89–98 (2013)
3. Blanchet, A., Dolbeault, J., Perthame, B.: Two-dimensional Keller-Segel model: optimal critical mass and qualitative properties of the solutions. Electron. J. Differ. Equ. **44**, 1 (2006)
4. Budrene, E.O., Berg, H.C.: Dynamics of formation of symmetrical patterns by chemotactic bacteria. Nature **376**(6535), 49–53 (1995)
5. Chertock, A., Kurganov, A.: A second-order positivity preserving central-upwind scheme for Chemotaxis and haptotaxis models. Numer. Math. **111**(2), 169–205 (2008)
6. Chertock, A., Kurganov, A., Ricchiuto, M., Wu, T.: Adaptive moving mesh upwind scheme for the two-species Chemotaxis model. Comput. Math. Appl. **77**(12), 3172–3185 (2019)
7. Conca, C., Espejo, E., Vilches, K.: Remarks on the blowup and global existence for a two species chemotactic Keller-Segel system in R^2. Eur. J. Appl. Math. **22**, 553–580 (2011)
8. Corrias, L., Perthame, B., Zaag, H.: Global solutions of some Chemotaxis and angiogenesis systems in high space dimensions. Milan J. Math. **72**, 1–28 (2004)
9. Dolak, Y., Schmeiser, C.: The Keller-Segel model with logistic sensitivity function and small diffusivity. SIAM J. Appl. Math. **66**(1), 286–308 (2005)

10. Espejo, E.E., Stevens, A., Velázquez, J.J.L.: Simultaneous finite time blow-up in a two-species model for Chemotaxis. Analysis **29**, 317–338 (2009)
11. Espejo, E.E., Stevens, A., Suzuki, T.: Simultaneous blowup and mass separation during collapse in an interacting system of chemotactic species. Differ. Integral Equ. **25**, 251–288 (2012)
12. Espejo, E.E., Vilches, K., Conca, C.: Sharp condition for blow-up and global existence in a two species chemotactic Keller-Segel system in R^2. Eur. J. Appl. Math. **24**, 297–313 (2013)
13. He, S., Tadmor, E.: Multi-species Patlak-Keller-Segel system. Indiana Univ. Math. J. **70**(4), 1578–1624 (2021)
14. Herrero, M.A., Velázquez, J.J.L.: Chemotactic collapse for the Keller-Segel model. J. Math. Biol. **35**(2), 177–194 (1996)
15. Hillen, T., Painter, K.J.: Global existence for a parabolic Chemotaxis model with prevention of overcrowding. Adv. Appl. Math. **26**(4), 280–301 (2001)
16. Hillen, T., Painter, K.J.: A user's guide to PDE models for Chemotaxis. J. Math. Biol. **58**(1), 183–217 (2009)
17. Horstmann, D.: From 1970 until present: the Keller-Segel model in Chemotaxis and its consequences I. Jahresber. Dtsch. Math.-Ver. **105**(3), 103–165 (2003)
18. Hu, J., Zhang, X.: Positivity-preserving and energy-dissipative finite difference schemes for the Fokker-Planck and Keller-Segel equations. IMA J. Numer. Anal. **43**(3), 1450–1484 (2023)
19. Huang, F., Shen, J.: Bound/positivity preserving and energy stable SAV schemes for dissipative systems: applications to Keller-Segel and Poisson-Nernst-Planck equations. Siam J. Sci. Comput. **43**(3) (2021)
20. Huang, F., Shen, J.: A new class of implicit-explicit BDFk SAV schemes for general dissipative systems and their error analysis. Comput. Methods Appl. Mech. Eng. **392**, 114718 (2022)
21. Huang, X., Shen, J.: Bound/positivity preserving SAV schemes for the Patlak-Keller-Segel-Navier-Stokes system. J. Comput. Phys. **480**, 112034 (2023)
22. Huang, X., Xiao, X., Zhao, J., Feng, X.: An efficient operator-splitting FEM-FCT algorithm for 3D Chemotaxis models. Eng. Comput. **36**, 1393–1404 (2020)
23. Jäger, W., Luckhaus, S.: On explosions of solutions to a system of partial differential equations modelling Chemotaxis. Trans. Am. Math. Soc. **329**(2), 819–824 (1992)
24. Jin, S., Lu, H., Pareschi, L.: A high order stochastic asymptotic preserving scheme for Chemotaxis kinetic models with random inputs. Multiscale Model. Simul. **16**, 1884–1915 (2018)
25. Keller, E.F., Segel, L.A.: Model for Chemotaxis. J. Theor. Biol. **30**(2), 225–234 (1971)
26. Kurganov, A., Lukacova-Medvidova, M.: Numerical study of two-species Chemotaxis models. Discrete Contin. Dyn. Syst., Ser. B **19**(1), 131 (2014)
27. Lankeit, J., Winkler, M.: Facing low regularity in Chemotaxis systems. Jahresber. Dtsch. Math.-Ver. **122**(1), 35–64 (2020)
28. Li, Y., Li, Y.X.: Finite-time blow-up in higher dimensional parabolic-parabolic Chemotaxis system for two species. Nonlinear Anal., Theory Methods Appl. **109**, 72–84 (2014)
29. Nagai, T.: Blowup of nonradial solutions to parabolic-elliptic systems modeling Chemotaxis in two-dimensional domains. J. Inequal. Appl. **6**, 37–55 (2001)
30. Patlak, C.S.: Random walk with persistence and external bias. Bull. Math. Biophys. **15**(3), 311–338 (1953)
31. Shen, J., Xu, J.: Unconditionally bound preserving and energy dissipative schemes for a class of Keller-Segel equations. SIAM J. Numer. Anal. **58**(3), 1674–1695 (2020)
32. Strehl, R., Sokolov, A., Kuzmin, D., Turek, S.: A fux-corrected fnite element method for Chemotaxis problems. Comput. Methods Appl. Math. **10**(2), 219–232 (2010)
33. Velázquez, J.J.L.: Point dynamics in a singular limit of the Keller-Segel model 1: motion of the concentration regions. SIAM J. Appl. Math. **64**(4), 1198–1223 (2004)
34. Velázquez, J.J.L.: Point dynamics in a singular limit of the Keller-Segel model 2: formation of the concentration regions. SIAM J. Appl. Math. **64**(4), 1224–1248 (2004)
35. Wang, S., Zhou, S., Shi, S., Chen, W.: Fully decoupled and energy stable BDF schemes for a class of Keller-Segel equations. J. Comput. Phys. **449**, 110799 (2022)
36. Wolansky, G.: Multi-components chemotactic system in the absence of conflicts. Eur. J. Appl. Math. **13**(6), 641–661 (2002)
37. Zhang, Y., Shen, J.: A generalized SAV approach with relaxation for dissipative systems. J. Comput. Phys. **464**, 111311 (2022)